LEGIBILITY NOTICE

A major purpose of the Technical Information Center is to provide the broadest dissemination possible of information contained in DOE's Research and Development Reports to business, industry, the academic community, and federal, state and local governments.

Although a small portion of this report is not reproducible, it is being made available to expedite the availability of information on the research discussed herein.

RESEARCH TRIANGLE INSTITUTE

DRL No. 209
DRD Line Item No. SE-4

DOE/JPL/956741--85/03

DE85 009519

COMPREHENSIVE SILICON SOLAR CELL COMPUTER MODELING

Quarterly Progress Report No. 3

549-2000

July 5, 1984, to December 4, 1984

M. F. Lamorte

Principal Investigator

JPL Contract No. 956741

RTI Project No. 415U-2850

"The JPL Low-Cost Silicon Solar Array Project is sponsored by the U.S. Government Department of Energy and forms part of the Solar Photovoltaic Conversion Program to initiate a major effort toward the development of low-cost solar arrays. This work was performed for the Jet Propulsion Laboratory, California Institute of Technology by agreement between NASA and DOE."

POST OFFICE BOX 12194 RESEARCH TRIANGLE PARK, NORTH CAROLINA 27709

ACKNOWLEDGMENT

Coding the solar cell analysis and debugging the program was provided by W. M. Yeager and is gratefully acknowledged.

TABLE OF CONTENTS

1.0 INTRODUCTION

In Quarterly Reports Nos. 1 and 2, the phenomena submodels and the method of solving the transport equations used in the simulation program were presented. In this Quarterly Report No. 3, the remaining phenomena submodels are presented and discussed.

2.0 OPTICAL ABSORPTION COEFFICIENT

2.1 Background

The behavior of the absorption coefficient is most important, along with bandgap and diffusion length, in designing high-efficiency solar cells. Moreover, because small changes in the absorption coefficient typically produce significant changes in the cell terminal characteristics. Experimental data for undoped silicon in the energy range of 1.1 to 4.0 eV at 77 and 300 K [1-4] is well documented. Data also have been reported in the range of 1.0 to 1.5 eV in the temperature range of 4.2 to 415 K [5,6], also for undoped material. Other data have been published for selected radiation wavelengths of 1.7 μm and 1.5 μm for undoped material over the temperature range of 300 to 1075 K and for a sample doped with 2×10^{18} cm^{-3} concentration over the same temperature range [7]. Still other data have been published for the impurity concentration range of 10^{19} cm^{-3} to 10^{21} cm^{-3}, in the energy range of 1.5 to 4.0 eV at 300 K [7,8]. Data at the bandedge and below are also available [9,10]. Analytical functions [11] representing absorption data as a function of photon energy in the energy range of 1.175 to 3.0 eV, using the Bardeen-Blatt-Hall relationship [12-14], have not

been useful because of disagreements with experimental data [1-4]. A more recent publication proposes an analytical relationship for undoped silicon which gives good agreement with experimental data at 77 and 300 K over the energy range of 1.1 to 3.1 eV, and for selected energy values at 20 and 415 K [15]. Moreover, a relationship has also been proposed to correct for the absorption coefficient in degenerately doped silicon at 300 K [7].

2.2 Optical Transition Processes

A number of optical absorption processes have been reported in semiconductor materials. Three of these are typically present in solar cell grade silicon. Two are related to indirect and direct optical transitions [15] in low-concentration materials, and a third that describes the contribution, to the absorption coefficient, by degenerately doped silicon [7]. Each of these is briefly described below.

The relationship to represent the three components of the absorption coefficient in silicon is given by

$$\alpha(h\nu,T,N) = \alpha_{ID}(h\nu,T) + \alpha_{d}(h\nu,T) + \alpha_{DEG}(N) \quad , \tag{2-1}$$

where the indirect (nonvertical) optical transition contribution is given by [15]

$$\alpha_{ID}(h\nu,T) = \sum_{\substack{i=1 \\ j=1}}^{2} C_i A_j \left[\frac{(h\nu - E_{Gj}(T) + E_{pi})^2}{E^{E_{pi}/kT} - 1} + \frac{(h\nu - E_{Gj}(T) - E_{pi})^2}{1 - e^{-E_{pi}/kT}} \right] \tag{2-2}$$

where the direct (vertical) optical transition contribution is given by [15]

Table 2.1 Parameters that appear in the absorption coefficient relationship, Eqs. (2-1)-(2-4)

Symbol	Value at OK	Relationship	Comments
E_{G1}	1.1557 eV	$E_{G1} = E_{G1}(0) - \frac{\beta G T^2}{T+\gamma_G} - (\Delta E_G)_{FD}$	Thermal bandgap - X_1 minima (100)
E_{G2}	2.5 eV	$E_{G2} = E_{G2}(0) - \frac{\beta G T^2}{T+\gamma_G} - (\Delta E_G)_{FD}$	L_1 minima (111)
E_{Gd}	3.2 eV	$E_{Gd} = E_{Gd}(0) - \frac{\beta G T^2}{T+\gamma_G} - (\Delta E_G)_{FD}$	direct transition
E_{p1}	1.827×10^{-2} eV		transverse acoustical phonon energy
E_{p2}	5.773×10^{-2} eV		transverse optical phonon energy
C_1	5.5		transverse acoustical coefficient
C_2	4.0		transverse optical coefficient
A_1	3.231×10^2 cm^{-1} $(eV)^{-2}$		X_1 indirect thermal bandgap coefficient
A_2	7.237×10^3 cm^{-1} $(eV)^{-2}$		L_1 indirect bandgap coefficient
A_d	1.052×10^6 cm^{-1} $(eV)^{1/2}$		Γ_{15} direct transition coefficient
K	1.8×10^{-15} cm^2 (As) 1.8×10^{-16} cm^2 (P,B)		As doping P and B doping
E_o	0.58 eV		
β_G	7.021×10^{-4} eV (K^{-1})		
γ_G	1108 K		

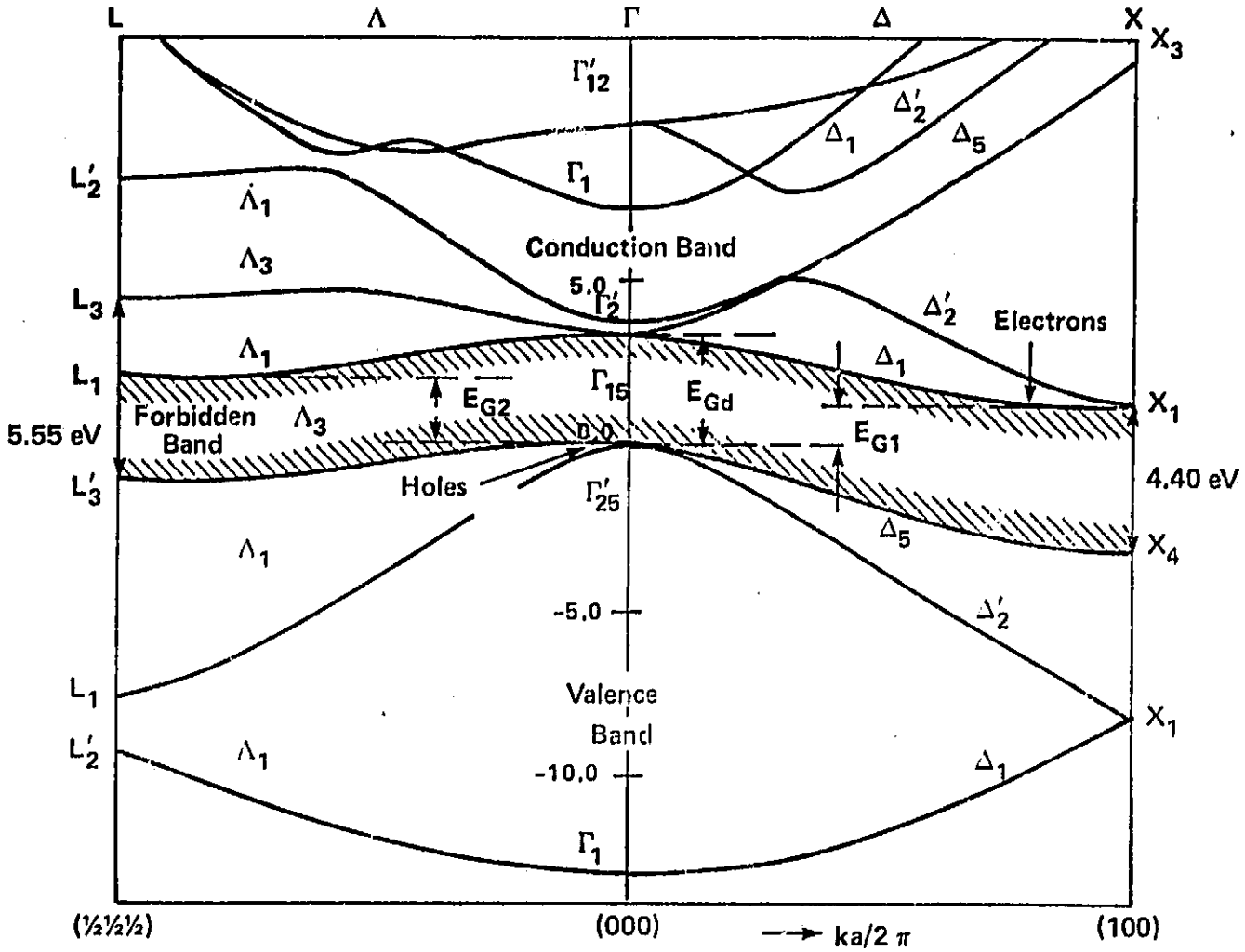

Figure 2-1. Energy band structure of silicon.

$$\alpha_d(h\nu,E_{Gd}) = A_d(h\nu - E_{Gd}(T))^{1/2} \quad , \tag{2-3}$$

and where the degenerate doping contribution is given by [7]

$$\alpha_{DEG}(N) = KNe^{\frac{h\nu - 3.4}{E_o}} \quad , \tag{2-4}$$

where N is the doping concentration and where the other parameters are defined and given in Table 2.1. Allowed transitions are represented by each of the absorption processes given in Eq. (2-1). In those cases where forbidden transitions also occur, the relationships for those processes must be added to the terms in Eq. (2-1).

Figure 2.1 shows the band structure for silicon. Indirect optical transitions may take place with band minima along the (100) and (111) orientations. The former is the thermal bandgap and is designated E_{G1}, while the latter is designated E_{G2}. Direct transitions occur between Γ_{25}' and Γ_{15}. While the indirect and direct transition processes are fairly well understood, the optical transitions contributed by degenerately doped silicon are not. One may speculate that Eq. (2-4) represents a number of optical processes that occur in degenerately doped silicon, including forbidden transitions which may play a significant role. In view of this conclusion, the effects of forbidden transitions may not need to be treated as a separate component.

For allowed indirect transitions, where absorption and emission of a phonon must be considered, consider two terms contained in Eq. (2-2) for the absorption coefficient given by

$$\alpha_{ija} + \alpha_{ije} = C_i A_j \left[\frac{(h\nu - E_{Gj} + E_{pi})^2}{e^{E_{pi}/kT} - 1} + \frac{(h\nu - E_{Gj} - E_{pi})^2}{1 - e^{-E_{pi}/kT}} \right] \quad . \qquad (2\text{-}5)$$

The subscript i identifies the phonon energy, E_{pi}, and j identifies the indirect bandgap minima. Relationships of the form given in Eq. (2-5) are defined only in the photon energy range for which

$$h\nu \geq (E_{Gj} \pm E_{pi}) \quad . \qquad (2\text{-}6)$$

In the case of silicon, Table 2.1 identifies two phonon energies, E_{p1} and E_{p2}, and two indirect conduction band minima, E_{G1} and E_{G2}, where E_{G1} is the thermal bandgap. Therefore, there are a total of four terms in Eq. (2-2) of the form shown in Eq. (2-5). From the relationships of Eqs. (2-2) and (2-6), it is clear that each of the eight terms in Eq. (2-2) exhibit a threshold for contributing to photon absorption in silicon. There is also a ninth threshold, $h\nu = E_{Gd}$, represented by the direct transition contribution given in Eq. (2-3). The threshold for the degenerate contribution, Eq. (2-4), is taken to be $h\nu = E_{G1} - E_{p2}$ which coincides with the lowest threshold photon energy represented in Eq. (2-2).

3.0 OPTIMUM GRID CONTACT DESIGN

3.1 Introduction

Series resistance and contact shadowing have been recognized as important parameters in the design of photovoltaic solar cells. Typically, the effects of series resistance on solar cell performance is considered in isolation [16-19] from the effects of shadowing [20]. Notwithstanding, the effects of series resistance and

contact shadowing produce competing effects and should not be studied as separate effects. If the grid contact stripes of a cell are designed for wide separation, contact shadowing is small, but Joule power loss may be excessive; on the other hand, narrow finger separation results in a small Joule power loss, but contact shadowing may be excessive. In either design, the efficiency of the cell may be increased by determining an optimum grid finger separation [21-23]. Although optimum finger separation studies that have been published [21-23] are useful, the accuracy of the methods are not commensurate with the accuracy of one-dimensional computer simulations.

The method used in this study follows the approach used in an early publication [21], but the present method does not make use of simplifying assumptions in order to obtain a convenient closed-form relationship which solution gives the optimum finger contact separation. This relationship is obtained by constructing the output power density for the solar cell and obtaining a relationship from setting the first derivative equal to zero. This approach differs significantly from the approach in which the Joule power loss is minimized. The latter may not result in maximum efficiency from the cell.

3.1 Analysis

Figure 3.1 shows a section of the solar cell structure under consideration and graphically identifies the parameters used in the analysis. Uniform incident photon flux and photocurrent generation in the x-y junction plane is assumed in those regions not shadowed by a grid finger contact. However, the current density flow vector, a short distance away on either side of the p-n junction, depends

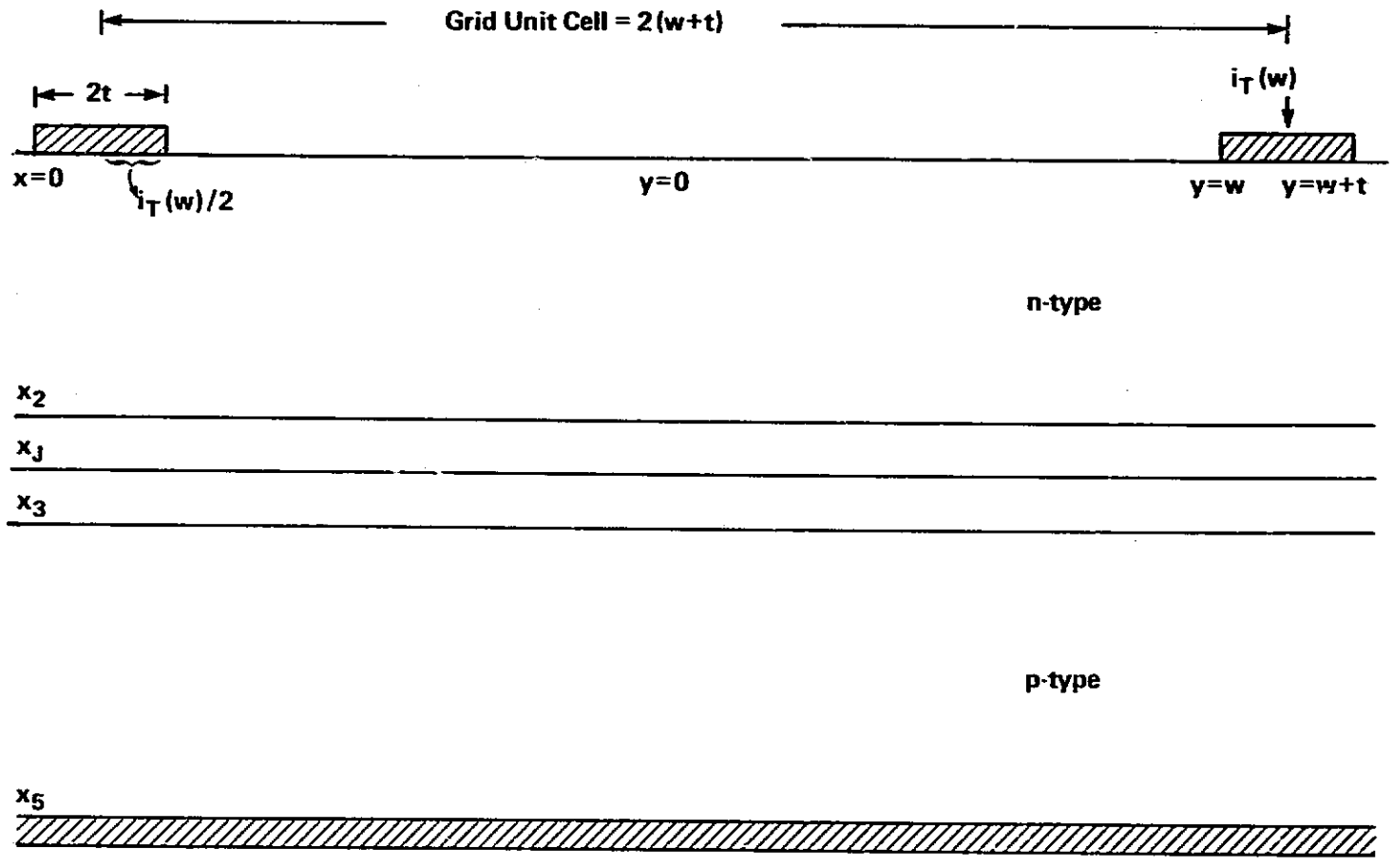

Figure 3-1. Cross section of grid unit cell (GUC).

strongly on the position relative to the finger contact. The photovoltage in the x-y junction plane is assumed to be independent of the y-position, even for those portions of the p-n junction that are shadowed. This eliminates from consideration circulating currents in the x-y junction plane. It follows from this assumption that the dark current contribution is uniform, even for those regions that are shadowed. The junction depth is assumed very small compared with typical finger separation distances. Grid finger electrodes are assumed to be equipotential surfaces; therefore, the voltage drop along the metal contact is vanishingly small. Lateral current is affected only by lateral electric field, as in ohms law, in which diffusion of carriers is negligibly small.

To facilitate the analysis, a "grid unit cell" (GUC) is defined in the surface plane, the boundaries of which are defined by $y = \pm(w + t)$. When the cell width is equal to W, the number of GUCs is given by

$$\varsigma = \frac{W}{2(w + t)} \quad . \tag{3-1}$$

The cell may then be represented by connecting as many GUCs to form the solar cell. Denoting $i_T(w)$ as the terminal current to represent each GUC, the total terminal current density, where $W = 1$ cm, is given by

$$J_T = \varsigma\, i_T(w) \quad . \tag{3-2}$$

Further, the analysis uses a distributed solar cell structure as shown in Figure 3.1 [21].

It is also assumed that the terminal current density, J_T, is accurately represented by the diode equation given by

$$J_T = J_{sc} - J_o(e^{V_T/AkT} - 1) \quad , \tag{3-3}$$

where the diode factor A may be greater than unity and in which both the diffusion and depletion region equivalent saturation current are represented by J_o. The short-circuit current density has been corrected for active area, whereas J_o and A are assumed to be uniform over the entire p-n junction plane. While J_o and A are made to represent the p-n junction at the p-n junction plane, the effect of current transport between the p-n junction plane and the grid finger and back contact is represented by the terminal voltage, V_T, given by

$$V_T = V_J - R_T J_T \tag{3-4}$$

where the diode total resistance is given by

$$R_T = \frac{\rho_n(x_2^2 + w^2)}{2x_2} + \frac{\rho_p(x_5 - x_3)}{2} + \frac{R_c}{\varsigma} \quad . \tag{3-5}$$

In Eq. (3-4), V_j is the p-n junction photovoltage generated across the depletion region surrounding the p-n junction, and R_c is the diode contact resistance contributed by both the top and bottom contacts in each GUC. The first term in Eq. (3-5) represents the resistance between the p-n junction plane and the grid finger contact, while the second is the corresponding resistance in the base region, and the third is the total contact resistance of the cell. The n- and p-type resistivities

are represented by ρ_n and ρ_p, respectively.

Applying the distributed solar cell to the GUC, the corresponding current is represented by

$$i_T(w) = 2\int_o^w \left[J_{sc} - J_o(e^{V(y)/AkT} - 1)\right] dy - 2\int_w^{w+t} J_o e^{V_T/AkT} dy \quad , \qquad (3\text{-}6)$$

where the grid finger length, 1, is taken to be 1 cm and $V_T(y)$ is represented by (3-4) but using a GUC resistance that is a function of y and given by

$$R_T(y) = \frac{\rho_n(x_2^2 + y^2)}{2x_2} + \frac{\rho_p(x_5 - x_3)}{2} + \frac{R_c}{\varsigma} \quad . \qquad (3\text{-}7)$$

Carrying out the operations in Eq. (3-6) results in the current expression

$$i_T(w) = aw - b + 2tJ_o - c\int_o^w e^{-\rho_n J_T y^2/(2x_2 AkT)} dy \quad , \qquad (3\text{-}8)$$

where

$$a = 2(J_{sc} + J_o) \quad , \qquad (3\text{-}9)$$

$$b = 2tJ_o\, e^{V_T/AkT} \quad , \qquad (3\text{-}10)$$

and

$$c = 2J_o e^{V_J - R_T(o)J_T)/AkT} \quad , \qquad (3\text{-}11)$$

while the first term in Eq. (3-6) is an integration of the photocurrent and dark current over the GUC that is not shadowed by the contact, the second term represents the dark current that is present under the contact areas.

Power density for the GUC is given by

$$P_{GUC} = \frac{i_T(w)V_T}{2(w + t)} \quad . \tag{3-12}$$

By setting the first derivative of P_{GUC} equal to zero, a relationship is obtained that contains w, of which the solution is its optimum value to maximize conversion efficiency, and is given by

$$\left[V_T - i_T(w)R_c\right] \frac{di_T(w)}{dw} - \left[\frac{V_T}{w + t} + \frac{\rho_n J_T w}{x_2}\right] i_T(w) = 0 \quad , \tag{3-13}$$

where

$$\frac{di_T(w)}{dw} = \frac{a + b\dfrac{\rho_n J_T w}{x_2 AkT} - ce^{-\rho_n J_T w^2/(2x_2 AkT)}}{1 - \dfrac{R_c}{AkT}\left[b + c\displaystyle\int_o^w e^{-\rho_n J_T y^2/(2x_2 AkT)} dy\right]} \quad . \tag{3-14}$$

Eq. (3-13) is a transcendental function in w. However, an iteration procedure must be used because $i_T(w)$, V_t, R_T, and $di_T(w)/dw$ must be updated for each trial value of w.

In the computer program, Newton's method is used to solve for w. In representing the left-hand side of Eq. (3-13) by f(w), the first two terms of the Taylor expansion is used from which the result is given by

$$w = w_o - \left\{\frac{d}{dw}\left[\ln f(w_o)\right]\right\}^{-1} \quad . \tag{3-15}$$

In Eq. (3-15), w_o is a trial value to determine if Eq. (3-13) is satisfied. If the absolute value of the right-hand side of Eq. (3-15) is greater than some predetermined value, w represents the next value of w_o that is to be substituted with Eq. (3-15). Iteration continues until the condition is satisfied.

REFERENCES

1. W. C. Dash and R. Newman, Phys. Rev., 99, 1151, (1955).

2. H. R. Philipp and E. A. Taft, Phys. Rev., 120, 37 (1960).

3. T. P. McLean, Progress in Semiconductors, Edited by A. F. Gibson, Vol. 5, p. 53, Wiley, New York (1960).

4. H. W. Brandhorst, Jr., NASA Lewis Res. Center, Private Communication (1976).

5. G. G. Macfarlane, T. P. McLean, J. E. Quarrington, and V. Roberts, Phys. Rev., 111, 1245 (1959).

6. G. G. Macfarlane, T. P. McLean, J. E. Quarrington, and V. Roberts, J. Phys. Chem. Solids, 8, 388 (1959).

7. G. E. Jellison, Jr., F. A. Modine, C. W. White, and R. T. Young, 15th IEEE Photovoltaic Specialists Conf. - 1981, 1164-1169, Kissimmee, Fla., May 12-15, 1981.

8. G. Lubberts and B. C. Burkey, J. Appl. Phys., 55, 760-763.

9. Victor I. Fistul, Heavily Doped Semiconductors, p. 229gg, Plenum Press, New York (1969).

10. D. I. Bilenko and V. D. Tsiporukha, Izvestiya Vysshikh Ucheknykh Zavedenii, Fizika, 10, 139-142, October 1974.

11. B. Bhaumik and R. Sharan, Appl. Phys. Lett., 29, 257 (1976).

12. J. Bardeen, F. J. Blatt, and L. H. Hall, Photoconductivity Conference, Atlantic City, Nov. 1954, Edited by R. G. Breckenridge, B. R. Russell, and E. E. Hahn, p. 146, Wiley, New York.

13. L. H. Ball, J. Bardeen, and F. J. Blatt, Phys. Rev., 96, 559 (1954).

14. F. J. Blatt, Physics of Electronic Conduction in Solids, p. 335, McGraw-Hill, New York (1968).

15. K. Rajkanan, R. Singh, and J. Shewchun, Solid-State Electronics, 22, 793-795, 1979.

16. M. Wolf, Proc. Inst. Radio Engrs, 48, 1246 (1960.

17. R. J. Handy, Solid-State Electronics, 10, 765-775, 1967.

18. G. M. Smirnov and J. E. Mahan, Solid-State Electronics, 23, 1055-1058, 1980.

19. D. K. Schroder and D. L. Meier, IEEE Trans. Elect. Devices ED-31, 637-647, 1984.

20. A. R. ES-Slassi, P. H. Nguiyen, J. Bottin, T. Easwarakhantan, and S. Ravelet, Electronics Lett., 20, 677-678, 1984.

21. M. F. Lamorte, Advanced Energy Conversion, 3, 551-563, 1963.

22. N. Convers Wyeth, Solid-State Electronics, 20, 629-634, 1977.

23. M. Conti, Solid-State Electronics, 24, 79-83, 1981.